

# On fatigue life predictions for notched members by the nominal stress-based and the local strain-based methods

J. A. R. Duran<sup>a,\*</sup>

<sup>a</sup>Mechanical Engineering Department, Volta Redonda School of Metallurgical Engineering, Federal Fluminense University, Brazil

Received 12 February 2021; accepted 24 February 2022

---

## Abstract

Traditional engineering models for addressing fatigue issues are based on empirical relations between the necessary number of cycles for fatigue failures  $N_f$  and either, the nominal stress  $\sigma_{an}$  or the local strain  $\varepsilon_a$  amplitudes. The aim of the present paper is to highlight the advantages of the local strain-based approach  $\varepsilon N$  for fatigue assessment of notched components over the more traditional stress-based approach  $\sigma N$ . Since a closed form solution for the ratio between fatigue life predictions among the two methods does not exist, we have considered a hypothetical case study that included variables such as the applied stress, the stress concentration factor and the structural material, and numerically calculated the expected fatigue life according to each approach. In order to highlight the differences related with the stress-strain analysis, the applied nominal stresses (uniaxial) were limited to the elastic region where both methods use approximately the same fatigue strength curve. Additionally a unique and equal function for accounting for the mean stress effects was incorporated in both approaches. Fatigue life predictions are expressed in universal graphs of normalized stress versus the  $N_f^{\text{ratio}}$ , the latter parameter defined as the quotient between the  $N_f$  predictions according to the  $\sigma N$  and  $\varepsilon N$  approaches, considering the average values for a group of sixty structural steels at each load level. The results confirm that fatigue life predictions under the traditional stress based approach are conservative when compared to the strain based approach for all the possible scenarios described by the variables involved.

© 2022 University of West Bohemia.

*Keywords:* strain based approach, Neuber's rule, SWT parameter

---

## 1. Introduction

Fatigue of metals under cyclic or vibratory loads is a well-known issue on modern machinery, despite huge research efforts spent over it since the 19th century. The cumulative character of the fatigue mechanisms is irreversible [21] and can lead to the nucleation of small fatigue cracks which can grow later and cause the total collapse of components or structures. Fatigue life assessment models can be broadly divided in two groups: those concerned with the predictions of the fatigue crack nucleation and those based on a fatigue damage parameter which is calculated on each cycle [18]. In the first group, a comparison between the stress/strain components and their respective strength curves is made. Additionally, variable amplitude load histories are addressed through a damage accumulation rule. The present paper focuses on these group of models.

Since the intrinsic characteristics of the fatigue cracks nucleation process are different from the fatigue crack growth process, different approaches have been developed in each stage [11]. In the engineering community, the most popular models in the nucleation phase are those based on nominal stresses (the  $\sigma N$  approach) or local strains analysis (the  $\varepsilon N$  approach). In

---

\*Corresponding author. Tel.: +55 24 992 615 529, e-mail: jorgeduran@id.uff.br.  
<https://doi.org/10.24132/acm.2022.678>

the crack propagation phase, the favorite model is based on linear elastic fracture mechanics *LEFM* (the  $da/dN$  vs.  $\Delta K$  approach) [9]. These methods were occasionally combined in the past. For example, models for fatigue crack growth were developed and tested from the strain-based approach [7]. A unified model, which is a combination of the strain-based and fracture mechanics-based approaches [15], was also proposed at that time. This unified model has been recently applied to welded structures [12]. Obviously, there are many examples of fatigue life assessment using the stress, strain and *LEFM* models individually. For example, in the case of notched specimens submitted to laboratory tests using a standardized helicopter load spectrum, all the aforementioned approaches have predicted fatigue lives with reasonable accuracy [10].

The objective of the present research is to graphically compare the fatigue life predictions according to the stress and strain based approaches. In this way, it is intended to highlight the advantages of the strain-based approach over the more traditional stress-based approach for fatigue life assessment.

## 2. Fatigue strength curves

Modern closed loop servo hydraulic machines allow the fatigue strength curves, for a given material, to be obtained under uniaxial load or strain control using standardized specimens. In the first case, the primary cause for the observed fatigue failures after  $N_f$  cycles (or the fatigue driving force) is believed to be the imposed completely reversed stress amplitude  $\sigma_a$ . When plotted in bi-logarithmic scales and in the finite life region, the relation between variables  $\sigma_a$  and  $N_f$  exhibits a linear behavior. A regression analysis of these experimental data returns the so-called materials properties  $\sigma'_f$  and  $b$ . The fatigue strength curve is therefore expressed as

$$S_a = \sigma'_f (2N_f)^b. \quad (1)$$

Note that a clear distinction between the stresses applied during the tests  $\sigma_a$  and those that represent the fatigue strength curve  $S_a$ , i.e., that depend on the material, has been made. In any case it should be thinking of them as local values and not as nominal ones. The parameter  $\sigma'_f$  is the failure stress in one reversal or the curve intercept in  $N_f = 0.5$  cycles, while  $b$  is the slope of the same curve. For an AISI 4340 steel, e.g., reported values are  $\sigma'_f = 1722$  MPa and  $b = -0.0958$  [5]. Some materials exhibit a rise in slope  $b$  of the curve described by (1), mainly above  $10^7$  cycles, bordering on  $b = 0$  in some cases, which has been interpreted as a fatigue limit  $S_e$ . More recent studies suggest that in the so-called giga-cycle fatigue regime ( $N_f \gg \approx 10^8$  cycles) the fatigue strength continues to decrease [17], in spite of the fact that the nucleation mechanism changes. Under very particular circumstances of dynamic loading, the fatigue design for a particular life  $N_f$  simply consists in comparing the nominal stresses acting on the component and scaled by a safety factor  $X_S$ , with the fatigue resistance expressed in the form of (1). These circumstances could be, for example, a situation of completely reversed uniaxial stresses of constant amplitude and no stress concentration. Of course, machine elements and structures are more frequently designed for situations other than these simple cases. Some modifications for including effects such as stress concentrations, mean stresses etc. are then mandatory. Many of these modifications were addressed in a previous paper [6].

Since fatigue crack nucleation is essentially a plasticity dominated process, a more realistic treatment of the problem could be done using strains instead of stresses. This is the essence of the strain-based approach for fatigue design. The fatigue strength curves using the  $\varepsilon N$  method are experimentally measured using standardized specimens and under uniaxial amplitude strain control  $\varepsilon_a$ . The number of fatigue cycles  $N_f$  for failure remains as the dependent variable. As

usual, a linear least-squares fit, separately performed to the elastic and plastic components of the total amplitude strains, derives into the so-called Coffin-Manson equation and its correlate material parameters, namely  $\epsilon'_f$  and  $c$ :

$$\epsilon_a = \frac{\sigma'_f}{E} (2N_f)^b + \epsilon'_f (2N_f)^c. \quad (2)$$

Once again, it is didactically interesting to separate the applied strains  $\epsilon_a$  (for measuring the curve) from the material's dependent strength values  $\epsilon_a$ . The tests for obtaining (2) are operationally more complicated than those performed under the traditional load control. However, the material properties obtained can better characterize the fatigue strength in the low-cycle fatigue *LCF* regime. It is also worth remembering that, in this regime, stresses can be considered as an ill-conditioned parameter for damage characterization, mainly for low hardening materials (e.g., see the non-linear term in the second line of the system of equations (8)). The equation (2) remains valid for multiaxial proportional loading as long as the effective strain and stress quantities are used instead [8].

### 3. Stress analysis and mean stress effects under the $\sigma N$ approach

Stress analysis under the  $\sigma N$  approach is totally developed in the elastic regime. The nominal stress amplitude  $\sigma_{an}$  is either calculated by elementary analytic formulas or by numerical techniques in more complex geometries. The mean stress has a detrimental effect on fatigue strength but the functions to take it into account are normally included in the stress analysis. The most popular of them include some monotonic or cyclic material property. One that is also widely used but does not rely in any material property was introduced by Smith et. al. [20] in 1970. The main idea behind this proposal is that the fatigue driving force encompasses two parameters, the maximum stress  $\sigma_{max}$  and the strain amplitude  $\epsilon_a$ , both of them being local ones. The geometric mean of these quantities represent a certain life function which would be valid for any mean stress. Putting this idea in a slightly different way we have

$$(\sigma_{max} \epsilon_a)_{\sigma N} \equiv g(N_f). \quad (3)$$

Since the product in (3) is proportional to the strain energy density, the so-called *SWT* (the initials of the authors) parameter can be viewed as an energetic approach. Furthermore, if the  $g(N_f)$  function is valid for any mean load, it will be valid for  $\sigma_m = 0$  as well. In the uniaxial situation  $\epsilon_a = \sigma_a/E$  and an equivalent, completely reverse stress amplitude  $\sigma_{ar}$  (or fatigue driving force corresponding to  $\sigma_m = 0$  in accordance with the *SWT* approach), can be defined as follows

$$\begin{aligned} \sigma_{max} \epsilon_a &= (\sigma_m + \sigma_a) \frac{\sigma_a}{E} = \frac{\sigma_{ar}^2}{E}, \\ \sigma_{ar}^2 &= \sigma_a^2 + \sigma_a \sigma_m. \end{aligned} \quad (4)$$

Of course, at the onset of fatigue failure it is expected that  $\sigma_{ar} = S_a$  or

$$g(N_f) = \frac{\sigma_{ar}^2}{E} = \frac{(\sigma'_f)^2 (2N_{f,\sigma N})^{2b}}{E}. \quad (5)$$

The equation (5) results from the combinations of (1) and (4). The success of this method can be evaluated, for example, if the scatter of a large set of experimental fatigue life data

for various combinations of amplitude and mean stress  $N_f(\sigma_a, \sigma_m)$ , for a given material, is notably reduced or, perhaps, eliminated, when plotted against the  $g(N_f)$  function. Conversely, for designing purposes, the fatigue life for any combination of the local values  $\sigma_a$  and  $\sigma_m$  can be found by substituting these values in (5) and solving for  $N_f$ .

Considering that the stress analysis under the  $\sigma N$  approach is purely elastic, the treatment for notched bodies simply consists in multiplying the nominal stresses by the elastic stress concentration factor  $K_t$  in order to obtain the local stress amplitudes. But since  $\sigma_{ar}$  is a local value we have

$$\sigma_{arn} = \frac{\sigma_{ar}}{K_t} \Rightarrow \sigma_{an}^2 + \sigma_{an} \sigma_{mn} = \frac{(\sigma'_f)^2 (2N_{f,\sigma N})^{2b}}{K_t^2}. \quad (6)$$

Differently from other linear mean stress equations widely used in fatigue analysis (e.g., Goodman or Morrow), under the *SWT* approach both, the nominal amplitude and the nominal mean stresses are multiplied by the same *SCF*, as can be seen in (6). Multiply the nominal mean stress by a  $K_t$  may result in undesirable  $\sigma_{\max}/S_y \geq 1$  relations and this issue will be addressed later in Section 5. A different  $K_{tm}$  which varies accordingly to the nominal maximum stress  $\sigma_{\max,n}$  is sometimes recommended for multiplying only the nominal mean stresses in brittle materials [4]. This suggestion, however, will not be followed in the present research since all the steels used in our simulation can be classified as ductile materials.

Solutions for *SCF* can be derived using analytic, numeric, or experimental tools. They are customarily presented in a non-dimensional form being, therefore, size independent. Stress concentration factors depend, however, on the notch geometry and type of loading. Departing from the point of the peak stress at the notch root surface, the stress gradient predicted from linear elastic solutions in a direction normal to the notch edge is higher than along the notch edge and these differences intensify for large  $K_t$  [19]. Since fatigue cracks nucleate mainly at the notch surface where constraint is less severe, notches with larger areas are more sensitive to the peak stresses defined by the  $K_t$ . This size effect is addressed with the help of a semi-empirical fatigue stress concentration factor  $K_f \leq K_t$ , defined as the ratio between the endurance limit in plain and notched specimens. Either in classical [14, 16] or modern [1, 3] formulations for notch sensitivity both, the material and notch geometry are invoked. But since notch geometry was not included among the variables in the present simulation, it was decided to use the  $K_t$  in its traditional form.

The predicted life, according to the stress-based approach  $N_{f,\sigma N}$ , can now be calculated by (6) for a given combination of nominal stress amplitude, mean stress and *SCF*.

#### 4. Mean stress effects and elastic-plastic stress strain analysis under the $\varepsilon N$ approach

The strain-life curves (see (2)) are also sensitive to mean loads. These effects are, however, introduced into the strain analysis in the  $\varepsilon N$  approach. The same mean load function, i.e., the *SWT* parameter will be used in order to include the influence of this variable in the present research. The logic behind the introduction of the  $P_{SWT}$  is similar to that previously used for stress-life curves. First note that under zero mean stress  $\sigma_m = 0 \rightarrow \sigma_{\max} = \sigma_{ar}$  and (3) reduces to

$$\begin{aligned} \sigma_{\max} \varepsilon_a &= \sigma_{ar} \varepsilon_{ar}, \\ (\sigma_{\max} \varepsilon_a)_{\varepsilon N} &\equiv h(N_f) = \frac{(\sigma'_f)^2}{E} (2N_{f,\varepsilon N})^{2b} + \varepsilon'_f \sigma'_f (2N_{f,\varepsilon N})^{b+c}. \end{aligned} \quad (7)$$

The second line in (7) results from the introduction of (1) and (2) under the consideration that, for fatigue failures to happen, applied loads must be enough to reach the measured strength values, i.e.,  $\sigma_{ar} = S_a$  and  $\varepsilon_{ar} = \varepsilon_a$ . Note that for small plastic strains, the rightmost term of the second line vanishes and (7) reduces to (5). Life calculations, according to the strain-based approach to obtain  $N_{f,\varepsilon N}$ , using the same combination of nominal stress amplitude, nominal mean stress and *SCF* used in the stress-based approach, can now proceed as long as the local values of  $\sigma_{\max}$  and  $\varepsilon_a$  of (7) are known. It is exactly at this point that major differences between the two approaches emerge. While in the  $\sigma N$  approach the local values are simply calculated by the use of the *SCF*, in the  $\varepsilon N$  approach a more refined, elastic-plastic analysis is performed.

New definitions are needed before proceeding. Since the monotonic (or the cyclic) stress-strain curve becomes non-linear once the plastic deformation begins at the notch root, the local stress  $K_\sigma$  and strain  $K_\varepsilon$  concentration factors must exhibit opposite trends. According to the Neuber [13] proposal, the geometric mean between these concentration factors equals the classical  $K_t$ . In addition, since the material behavior under cyclic loading must follow the path described by its constitutive  $\varepsilon_a = f(\sigma_a)$  relation in  $\sigma_a$  vs.  $\varepsilon_a$  coordinates, the desired local values for  $\sigma_a$  and  $\varepsilon_a$  must satisfy simultaneously the following system of two non-linear equations

$$\begin{aligned} \varepsilon_a \sigma_a &= \frac{(K_t \sigma_{an})^2}{E}, \\ \varepsilon_a &= \frac{\sigma_a}{E} + \left(\frac{\sigma_a}{H'}\right)^{\frac{1}{n'}}. \end{aligned} \tag{8}$$

The parameters with prime as superscripts in (8) indicate cyclic properties while  $E$  is the modulus of elasticity. It is numerically efficient, for solving (8), to first eliminate the  $\varepsilon_a$  between the two equations and calculate by iteration the  $\sigma_a$  for a given  $\sigma_{an}$  and  $K_t$ . The result is then substituted back in any of the two original equations to obtain  $\varepsilon_a$ . The system in (8) can also be solved for maximum local values ( $\varepsilon_{\max}$  and  $\sigma_{\max}$ ) simply replacing the subscripts  $a$  for  $\max$ . Since the same material's cyclic properties are used in the new system, it is implied that the material follows the cyclic stress strain curve since the first cycle of loading

$$\begin{aligned} \varepsilon_{\max} \sigma_{\max} &= \frac{(K_t \sigma_{\max,n})^2}{E}, \\ \varepsilon_{\max} &= \frac{\sigma_{\max}}{E} + \left(\frac{\sigma_{\max}}{H'}\right)^{\frac{1}{n'}}. \end{aligned} \tag{9}$$

Once the  $\varepsilon_a$  and  $\sigma_{\max}$  values are calculated, they are entered into (7) to finally calculate the fatigue life  $N_{f,\varepsilon N}$  by the  $\varepsilon N$  approach.

In order to clarify even more these ideas, a numerical example follows. Let a nominal stress history of constant amplitude  $\sigma_{an} = 143$  MPa ( $R = -1/2$ ) be applied in a notched component ( $K_t = 3$ ) of a material with  $E = 197$  GPa,  $H' = 1189$  MPa and  $n' = 0.15$ . Fig. 1a shows schematically the points of intersection between each pair of (8) and (9) in a common locus  $\varepsilon \sigma$ . The calculated local strain and stress values were  $\varepsilon_a = 2.5 \cdot 10^{-3}$  and  $\sigma_{\max} = 447$  MPa. The figure also shows the solutions based on the stress-based approach, whose numerical values are  $\sigma_a = K_t \sigma_{an} = 429$  MPa and  $\sigma_{\max} = K_t \sigma_{\max,n} = 2 K_t \sigma_a / (1 - R) = 572$  MPa. Of course, these solutions are based on the Hooke's law and do not have any relation with the Neuber's rule. The points  $\sigma = K_t \sigma_n$  also satisfy simultaneously the systems in (8) and (9) and this explains their graphical coincidence in Fig. 1a. This can be easily verified if the Ramberg-Osgood is replaced by the Hooke's law in any of the aforementioned systems of equations.

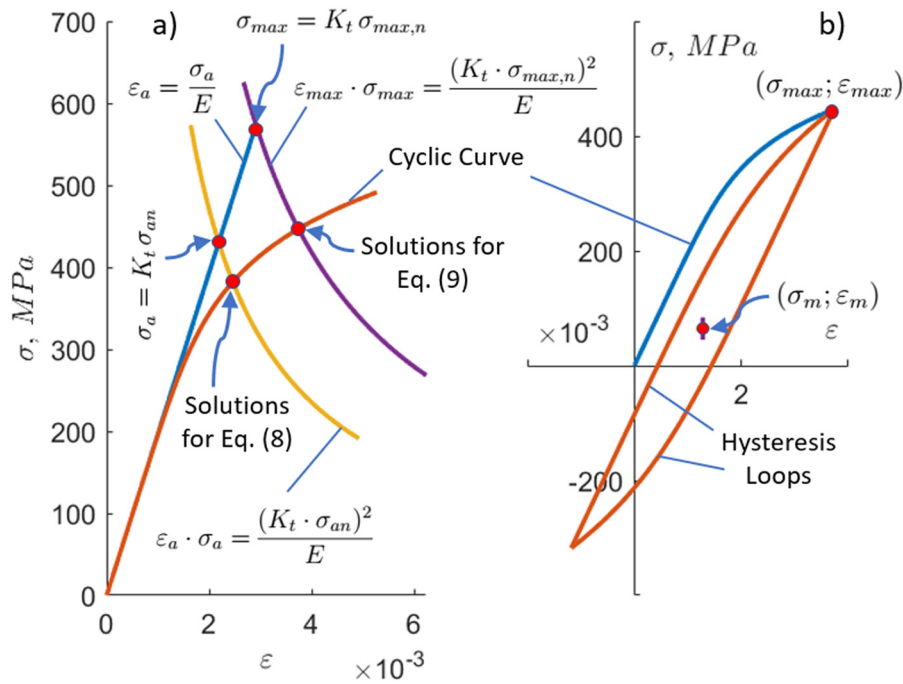


Fig. 1. (a) The constitutive curve for a AISI 1144 (199HB) steel (both cyclic according to the Ramberg-Osgood equation and linear elastic according to the Hooke's law) and (b) the hysteresis loops at the notch root using the strain-based approach solutions

Despite not necessary for life calculations, a plot of the true local stress strain paths (hysteresis loops) at the notch root, along with the initial monotonic response (here considered as equal to the cyclic stress strain curve, as stated before), is useful for visualization purposes (see Fig. 1b).

The (stabilized) hysteresis loops shown in Fig. 1b are mathematically described in the  $\Delta\varepsilon$ - $\Delta\sigma$  locus by a Ramberg-Osgood type relation

$$\Delta\varepsilon = \frac{\Delta\sigma}{E} + 2 \left( \frac{\Delta\sigma}{2H'} \right)^{1/n'} \quad (10)$$

The equation (10) describes curves departing from the loops tips. In  $\varepsilon$ - $\sigma$  coordinates the loading and unloading branches of the hysteresis loops, respectively, are given by

$$\begin{aligned} \varepsilon &= \varepsilon_{\min} + \Delta\varepsilon(\sigma - \sigma_{\min}), \\ \varepsilon &= \varepsilon_{\max} - \Delta\varepsilon(\sigma_{\max} - \sigma). \end{aligned} \quad (11)$$

## 5. Methodology for comparing the fatigue life predictions by the $\sigma N$ and $\varepsilon N$ approaches

Fatigue life predictions in the context of the  $\varepsilon N$  approach can only be obtained after solving numerically three equations. First, equations (8) and (9) must be solved for amplitudes and for maximum values, respectively. The results are entered in (7) which also requires a numerical iterative process to finally calculate the desired fatigue life  $N_{f,\varepsilon N}$ . For this reason, a closed form equation relating the fatigue life predictions according to the two methods, is not possible. In order to perform a numerical comparison, a hypothetical design or assessment case consisting of a notched structural member under uniaxial loading (Fig. 2) has been considered. Information relative to loading parameters, stress concentration factor and material are mandatory for this simulation.

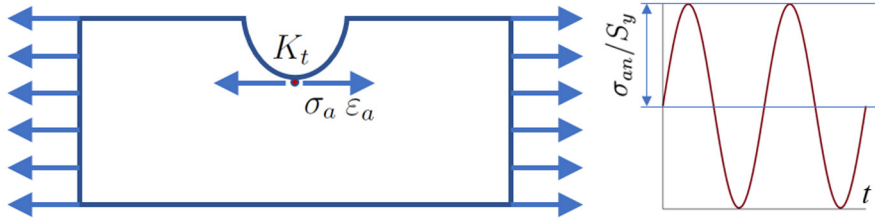


Fig. 2. Scheme of the generic notch used as a case study

In relation to the load, a vector of constant nominal stress amplitudes  $\sigma_{an}$  normalized with respect to the material's yield strength  $S_y$  in such a way that  $1/10 = 0.1 \leq \sigma_{an}/S_y \leq 0.2 = 1/5$  was applied to the member in Fig. 2. In order to avoid local yielding at the notch root, the local maximum notch stress to material's yield strength relation was limited to 0.8 or  $\sigma_{\max}/S_y = K_t \sigma_{\max,n}/S_y = 4/5$ . Consequently, a complete definition of the applied cyclic stresses is subordinate to the knowledge of the maximum *SCF* to be used. In our simulation the stress concentration factors vary in the range  $1.5 \leq K_t \leq 3$ . For constant stress amplitude cycles, the following relation holds between nominal quantities and also the load ratio  $R = \sigma_{\min,n}/\sigma_{\max,n}$

$$\sigma_{\max,n} = \frac{2\sigma_{an}}{1-R}. \quad (12)$$

The load ratio  $R$  necessary for keeping the maximum value of the local applied stress cycles below 80% of the yield strength, i.e., the parameter we were looking for, becomes a dependent variable of the maximum *SCF*. Substituting the upper limit of the load relation  $\sigma_{an}/S_y = 1/5$  in (12) and manipulating gives

$$\begin{aligned} \sigma_{\max} &= K_t \sigma_{\max,n} = K_t \frac{2\sigma_{an}}{(1-R)} = K_t \frac{2S_y}{5(1-R)}, \\ \frac{\sigma_{\max}}{S_y} &= \frac{2K_t}{5(1-R)} = \frac{4}{5} \Rightarrow R = 1 - \frac{K_t}{2}, \end{aligned} \quad (13)$$

which for  $K_t = 3$  gives  $R = -1/2$ . In relation to the material, we have gathered the monotonic and cyclic properties of 60 ductile structural steels [2]. These properties were used as input parameters in specially developed codes that implement the two methodologies described in the present paper. For each material, level of normalized load and *SCF*, the average value of the ratio between the  $\sigma N$  and  $\epsilon N$  life predictions, defined as the  $N_f^{\text{ratio}}$ , as well as other important quantities, were calculated and stored in appropriate data types.

## 6. Results and discussion

Fig. 3 shows the average  $N_f^{\text{ratio}}$  versus the normalized stresses for a group of 60 steels. The traditional and almost totally empirical stress based approach, returns conservative results (as compared to those provided by the strain based method) across the whole stress spectrum. The predicted life ratio is lower as the  $K_t$  increases. We should remember that only theoretical elastic values are present at the notch root (Section 5) so these results cannot be attributed to the obvious advantages of the strain-based approach over the stress-based approach for dealing with elastic-plastic values. We can use, however, Fig. 1a for a first explanation of the results. A Ramberg-Osgood type equation (second line in (8), orange line in Fig. 1a), here used for representing the material's cyclic curve, does not constitute a physical law, but a convenient

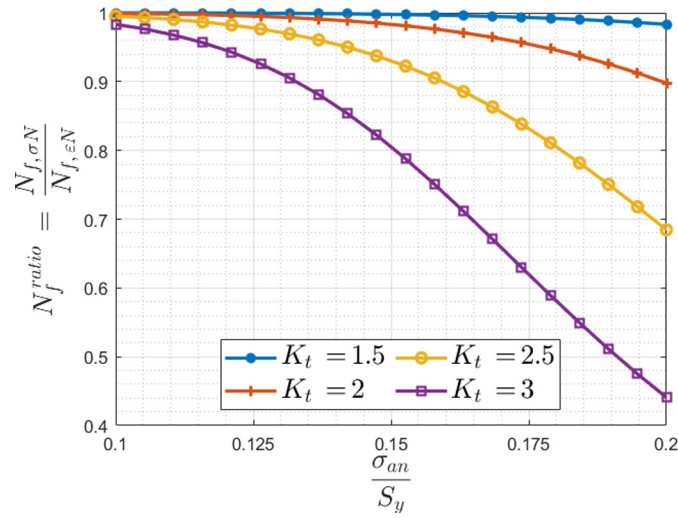


Fig. 3. Mean values of the ratio between life predictions from the  $\sigma N$  approach to the  $\varepsilon N$  approach for a group of 60 ductile structural steels for various normalized stress levels and stress concentration factors

mathematical way for fitting experimental values of stresses and strains amplitudes obtained, for example, in a low-cycle fatigue test. The Ramberg-Osgood relationship asymptotically approximates (i) a purely elastic behavior  $\varepsilon_a = \sigma_a/E$  at lower stresses and (ii) a predominantly elastic-plastic behavior  $\varepsilon_a = (\sigma_a/H')^{1/n'}$  at high stresses. Of course, since the upper bound of the load vector used in the present simulation was  $\sigma_{\max}/S_y \leq 4/5$ , the constitutive equation and the Hooke's law are very close but do not perfectly match. But since the fatigue driving forces  $\sigma_{\max} \varepsilon_a$  for the  $\varepsilon N$  and for the  $\sigma N$  approaches are based on the Ramberg-Osgood curve and on the Hooke's law, respectively, the main reason for the differences between the predictions are due to the imperfect match between these curves in the elastic region, enhanced by the strongly non linear character of the  $\sigma_{\max} \varepsilon_a$  versus  $N_f$  relationship.

Since either the numerical or analytic solutions can be graphically visualized in  $(\sigma_{\max} \varepsilon_a)$  vs.  $N_f$  coordinates, it is noteworthy to go deeper into this aspect. The fatigue strength curves  $g(N_f)$  and  $h(N_f)$  have been previously defined in (5) and (7), respectively. The loading points, in the other hand, are functions of the normalized load and stress concentration factor, i.e.,  $\sigma_{\max} \varepsilon_a = f(\sigma_{an}/S_y, K_t, R)$ . For a given material and specific values of these two parameters, a plot of the loading points along with the fatigue strength curves, can help explain the general trends observed in Fig. 3. This is done in Fig. 4 for two representative combinations of load and SCFs (see Table 1). Note that not only is the curve  $g(N_f)$  always to the left of  $h(N_f)$  but also the elastic-plastic analysis, although approximate, performed through (8) gives consistently lower values of the local driving force  $\sigma_{\max} \varepsilon_a$  than those obtained by (6). Of course, both factors contribute to the longer fatigue lives calculated under the  $\varepsilon N$  approach and explain the trends on  $N_f^{\text{ratio}}$  showed in Fig. 3.

Table 1. Parameters used for the loading points  $P_1, \dots, P_4$  showed in Fig. 4

$K_t$	$\sigma_{an}/S_y$	$(\sigma_{\max} \varepsilon_a)_{\sigma N} = \sigma_{ar}^2/E$	$(\sigma_{\max} \varepsilon_a)_{\varepsilon N}$
2	0.11	$P_1$	$P_2$
3	0.17	$P_3$	$P_4$

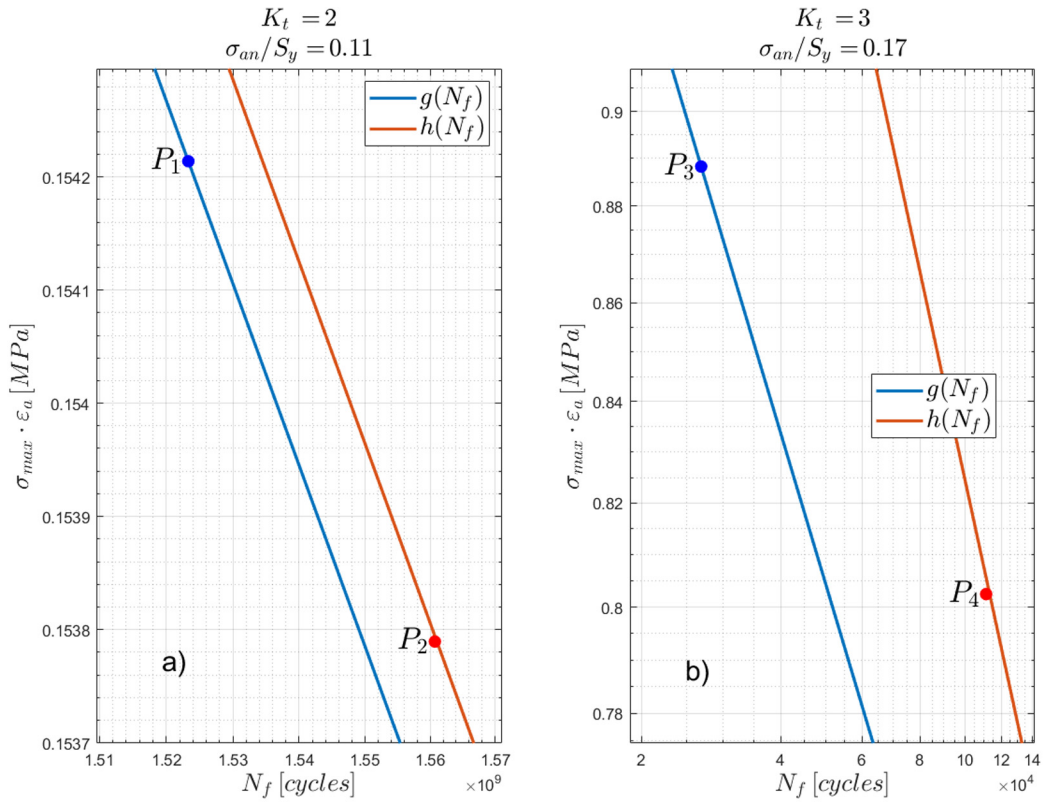


Fig. 4. Fatigue strength curves for the AISI 1144 (199 HB) steel according to (5) and (7). The loading points for (a)  $K_t = 2$ ,  $\sigma_{an}/S_y \approx 0.12$  and (b)  $K_t = 3$ ,  $\sigma_{an}/S_y \approx 0.21$  (first and second row in Table 1, respectively) are also shown in the figure

Fig. 5 shows the predicted hysteresis loops according to the  $\varepsilon N$  approach for four normalized load levels, material and stress concentration factor. The first and the third load levels are the same used before in Table 1. The material considered for the graph in Fig. 5 was again the

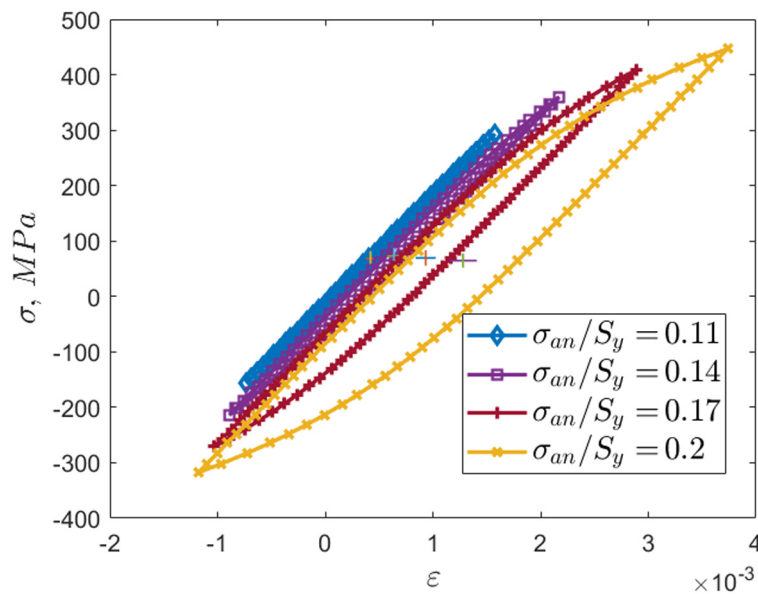


Fig. 5. Predicted hysteresis loops at the notch root ( $K_t = 3$ ) for different load levels. The extreme values at each load level were estimated by the solution of (8) and using the material’s properties for the AISI 1144 (199 HB) steel

AISI 1144 (199 HB) with a  $K_t = 3$ . The normalized load levels used, along with the center point in each hysteresis loop, i.e., the mean stress and strain calculated under the  $\varepsilon N$  method, are shown in the figure. After a initial increase, a slight tendency to decrease in the calculated local mean stress can be observed. On the other hand, the thicker the loops, the greater the plastic strain energy accumulated in the material. But since the fatigue driving force under the  $\varepsilon N$  approach is also related to the strain energy density (see (7)), Fig. 5 alone cannot explain the differences between the loading points in Fig. 4.

The aforementioned behavior and also that observed in Fig. 3, can be clarified if the trends in the estimated local mean stresses as the normalized load grows for a given stress concentration factor and material, are plotted as in Fig. 6a. The calculated mean stresses are normalized with relation to its value in the lower bound of the normalized load, i.e., to  $\sigma_m(\sigma_{an}/S_y = 0.1)$ . The curves for case (a) in Fig. 6 use the same combination of material and  $K_t$  that in previous figures, i.e., AISI 1144 (199 HB) and  $K_t = 3$ . The case (b) in the same figure reflects the local  $\sigma_m$  trends considering the arithmetic mean for the whole set of materials. The curve in blue ( $\sigma N$  method) remains the same in both parts of Fig. 6 because the dependence on the  $S_y$  is eliminated as a result of the normalization process. In both cases, the mean stress, calculated under the  $\sigma N$  approach, doubles its value because this component is simply related to the applied loads through  $\sigma_m = (1 + R)/(1 - R) K_t \sigma_{an}$ . The physically expected trend is the one predicted by the  $\varepsilon N$  approach, i.e., the trend to decrease the calculated mean stresses as the local yielding advances. In favor of the  $\sigma N$  approach, it should not be forgotten that only peak stresses, i.e., purely  $K_t \sigma_n$  stresses were considered, and in the absence of details related with the notch geometry, no attempt was made to include engineering methods for dealing with the notch sensitivity.

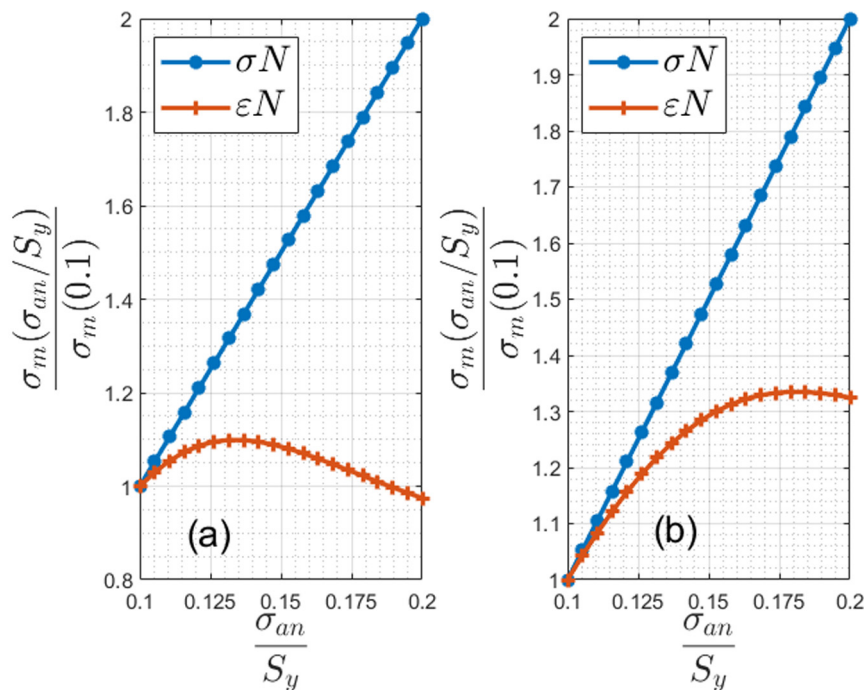


Fig. 6. (a) The calculated local mean stress (normalized in relation to the its first value) at different load levels for the AISI 1144 (199 HB) and using  $K_t = 3$  and (b) for the whole set of materials used in the present simulation

## 7. Conclusions

A simple comparison of (1) and (2) suggests that fatigue life predictions made under the  $\sigma N$  and  $\varepsilon N$  approaches, for predominantly elastic stresses, should tend to be effectively the same. This can be true for unnotched components and as long as the static component is zero. The simulation performed in the present work demonstrated that the fatigue life predictions by the stress-based approach, for notched parts and also in the presence of mean stresses, which were here addressed by the *SWT* parameter, are always conservative when compared to the strain-based approach. The strain based approach attempts to model the physics of the fatigue crack nucleation and its subsequent propagation on the order of various grains, perhaps until a size of around 1.0 mm is reached by the growing crack, and the results of the present research confirm this statement.

## References

- [1] Atzori, B., Lazzarin, P., Meneghetti, G., Fracture mechanics and notch sensitivity, *Fatigue & Fracture of Engineering Materials & Structures* 26 (3) (2003) 257–267. <https://doi.org/10.1046/j.1460-2695.2003.00633.x>
- [2] Boller, C., Seeger, T., Materials data for cyclic loading, Elsevier Science, Netherlands, Materials Science Monographs 42A, 1987.
- [3] de Castro, J. T. P., Meggiolaro, M. A., de Oliveira Miranda, A. C., Wu, H., Imad, A., Benseddiq, N., Prediction of fatigue crack initiation lives at elongated notch roots using short crack concepts, *International Journal of Fatigue* 42 (2012) 172–182. <https://doi.org/10.1016/j.ijfatigue.2011.10.010>
- [4] Dowling, N. E., Mechanical behavior of materials: Engineering methods for deformation, fracture and fatigue, 4th edition, Pearson Education Limited, 2013.
- [5] Dowling, N. E., Calhoun, C. A., Arcari, A., Mean stress effects in stress-life fatigue and the Walker equation, *Fatigue & Fracture of Engineering Materials & Structures* 32 (2009) 163–179. <https://doi.org/10.1111/j.1460-2695.2008.01322.x>
- [6] Duran, J., da Costa, D., An evaluation of the nominal stress method for life prediction of cylindrical circumferential V-notched specimens tested under variable amplitude loading, *Applied Mechanics and Materials* 851 (2016) 310–316. <https://doi.org/10.4028/www.scientific.net/AMM.851.310>
- [7] Duran, J. A. R., Castro, J. T., da Cruz Payão Filho, J., Fatigue crack propagation prediction by cyclic plasticity damage accumulation models, *Fatigue & Fracture of Engineering Materials & Structures* 26 (2003) 137–150. <https://doi.org/10.1046/j.1460-2695.2003.00630.x>
- [8] Duran, J. A. R., Costa, D. J. R. d., Ribeiro Junior, L. C. d. A., Numerical stress-life curves for the AISI 4340 steel using two sets of materials properties and different bi-axial stress ratios, *Latin American Journal of Solids and Structures* 15 (2018). <https://doi.org/10.1590/1679-78254308>
- [9] Duran, J. A. R., Hernandez, C. T., Evaluation of three of the current methods for including the mean stress effect in fatigue crack growth rate prediction, *Fatigue & Fracture of Engineering Materials & Structures* 38 (4) (2014) 410–419. <https://doi.org/10.1111/ffe.12242>
- [10] Everett, R., A comparison of fatigue life prediction methodologies for rotorcraft, Technical report, NASA Technical Memorandum 102759, 1990.
- [11] Kopas, P., Saga, M., Baniari, V., Vasko, M., Handrik, M., A plastic strain and stress analysis of bending and torsion fatigue specimens in the low-cycle fatigue region using the FEM, *Procedia Engineering* 177 (2017) 526–531. <https://doi.org/10.1016/j.proeng.2017.02.256>
- [12] Mikheevskiya, S., Glinka, G., Cordes, T., Total life approach for fatigue life estimation of welded structures, *Procedia Engineering* 101 (2015) 177–184. <https://doi.org/10.1016/j.proeng.2015.02.023>

- [13] Neuber, H., Theory of stress concentration for shear-strained prismatic bodies with nonlinear stress-strain law, *Journal of Applied Mechanics* 28 (4) (1961) 544–550. <https://doi.org/10.1115/1.3641780>
- [14] Neuber, H., Brock, J., Taylor, D. W., Theory of notch stresses: Principles for exact stress calculation, J. W. Edwards, 1946.
- [15] Noroozi, A., Glinka, G., Lambert, S., A two parameter driving force for fatigue crack growth analysis, *International Journal of Fatigue* 27 (2005) 1277–1296. <https://doi.org/10.1016/j.ijfatigue.2005.07.002>
- [16] Pilkey, W., Pilkey, D., Peterson's stress concentration factors, 3rd edition, John Wiley & Sons Inc, 2008. <https://doi.org/10.1002/9780470211106>
- [17] Sadananda, K., Vasudevan, A., Phan, N., Analysis of endurance limits under very high cycle fatigue using a unified damage approach, *International Journal of Fatigue* 29 (2007) 2060–2071. <https://doi.org/10.1016/j.ijfatigue.2007.02.028>
- [18] Santecchia, E., Hamouda, A. M. S., Musharavati, F., Zalnezhad, E., Cabibbo, M., El Mehtedi, M., Spigarelli, S., A review on fatigue life prediction methods for metals, *Advances in Materials Science and Engineering* 2016 (2016) 1–27. <https://doi.org/10.1155/2016/9573524>
- [19] Schijve, J., Stress gradients around notches, *Fatigue & Fracture of Engineering Materials & Structures* 3 (4) (1980) 325–338. <https://doi.org/10.1111/j.1460-2695.1980.tb01382.x>
- [20] Smith, K. N., Watson, P., Topper, T. H., A stress-strain function for the fatigue of metals, *Journal of Materials* 5 (4) (1970) 767–778.
- [21] Suresh, S., *Fatigue of materials*, Cambridge University Press, 2012.